Matter and Radiation at Extremes | RESEARCH ARTICLE | scitation.org/journal/mre

Free-surface velocity measurements of opaque materials in laser-driven shock-wave experiments using photonic Doppler velocimetry

Cite as: Matter Radiat. Extremes 6, 046902 (2021); doi: 10.1063/5.0046884
Submitted: 8 February 2021 • Accepted: 7 May 2021 •
Published Online: 8 June 2021

N. Nissim,[a] E. Greenberg, M. Werdiger, Y. Horowitz, L. Bakshi, Y. Ferber, B. Glam, A. Fedotov-Gefen, L. Perelmutter, and S. Eliezer

AFFILIATIONS

Applied Physics Division, Soreq NRC, Yavne, Israel

Note: This paper is part of the Special Issue on Matter in Extreme States Created by Laser.
[a]**Author to whom correspondence should be addressed:** noaznissim@gmail.com

ABSTRACT

We present a novel photonic Doppler velocimetry (PDV) design for laser-driven shock-wave experiments. This PDV design is intended to provide the capability of measuring the free-surface velocity of shocked opaque materials in the terapascal range. We present measurements of the free-surface velocity of gold for as long as ~2 ns from the shock breakout, at pressures of up to ~7 Mbar and a free-surface velocity of 7.3 km/s with an error of ~1.5%. Such laboratory pressure conditions are achieved predominantly at high-intensity laser facilities where the only velocity diagnostic is usually line-imaging velocity interferometry for any reflector. However, that diagnostic is limited by the lower dynamic range of the streak camera (at a temporal resolution relevant to laser shock experiments) to measure the free-surface velocity of opaque materials up to pressures of only ~1 Mbar. We expect the proposed PDV design to allow the free-surface velocity of opaque materials to be measured at much higher pressures.

I. INTRODUCTION

Photonic Doppler velocimetry (PDV) is intended for measuring the velocities of moving surfaces[1] and is often used in studying the equation of state (EOS) of materials in dynamic experiments.[2] PDV is usually used in the most common techniques for shockwave experiments, such as those based on guns[3,4] and explosives,[5] but it is seldom used with high-intensity laser experiments that can span the largest thermodynamic range and up to gigabar pressures.

There are a few approaches for measuring the thermodynamic conditions of the target in shock-wave experiments. (1) Placing the target material on top of a standard material.[6] The standard material is one that was previously calibrated and its EOS is known relatively well in the vicinity of the experimental conditions. By measuring the shock-wave velocity in the standard and target materials, the EOS of the target material can be extracted by using the impedance-mismatch technique and the reflected shock approximation (RSA). (2) Without using a reference material.[6] In this case, it is necessary to measure both the shock and particle velocities in the target material. Because measuring the particle velocity is a difficult task, a common technique is to measure the free-surface velocity and use the RSA method to extract the particle velocity. In that case, it is customary to use the approximation $u_{fs} \approx 2u_p$, i.e., that the free-surface velocity is twice the particle velocity.

Although it has been found in many experiments that the approximation $u_{fs} \approx 2u_p$ holds (within 1%) for many materials up to ~1 Mbar (i.e., $u_p \ll u_s$, where u_s is the shock velocity),[6] data are scarce regarding the maximum pressure at which this approximation still holds for different materials. In general, we have[6]

$$u_{fs} = u_p + u_r, \tag{1}$$

where u_r is the rarefaction wave velocity defined as

$$u_r = \int_{V(P_H)}^{V(P=0)} \left(-\frac{dP_S}{dV}\right)^{1/2} dV, \tag{2}$$

where P_H is the shock pressure, V is the specific volume, and P_S is the pressure along the release isentrope from the shock pressure to zero pressure.

As indicated by Eqs. (1) and (2), the combined measurement of u_{fs} and u_p holds important information about the EOS of materials at elevated pressures.

In laser-induced shock experiments, the measurement time scale is of the order of several nanoseconds, during which the optical reflectivity of the sample can change by several orders of magnitude. Usually in laser-shocked opaque materials, there is a large decrease in the free-surface reflectivity during the shock breakout. The most common velocimetry system for laser shock experiments to date is the Line-imaging Velocity Interferometer for any Reflector (Line-VISAR).[7,8] However, as a detector, the Line-VISAR technique uses a streak camera with a relatively small dynamic range, usually 10–100. Therefore, the free-surface velocity of opaque materials can typically be measured up to shock pressures of only ~1 Mbar.[9] By contrast, PDV can use an ultrafast photodiode as a detector and so can have a dynamic range larger than 10 000.[10] This provides PDV with an advantage in measuring the free-surface velocity of opaque materials in laser shock experiments.

Each of the experimental methods presented above has advantages and disadvantages. Herein, we focus on developing a specialized PDV for measuring the free-surface velocity of opaque materials in the pressure range of several megabars in laser-induced shock-wave experiments.

II. STANDARD PHOTONIC DOPPLER VELOCIMETRY

PDV is based on interference between two channels: (i) a reference channel with a fixed frequency v_r ($\omega_r = 2\pi v_r$), and (ii) a target channel that has a known initial frequency v_{ti} ($\omega_{ti} = 2\pi v_{ti}$) and undergoes a Doppler shift to $v_t(t)$ [$\omega_t(t) = 2\pi v_t(t)$] when it is reflected from a moving surface, i.e., the target. By measuring the frequency change $\Delta v_t(t) = |v_{ti} - v_t(t)|$ in the target channel, the target's velocity can be calculated. Because measuring the Doppler shift of the target channel through a direct measurement of the laser frequency is out of the reach of current detectors, the interference between the reference and target channels is used to create a beating pattern that can be detected by a fast detector and a high-sampling-rate oscilloscope. The intensity of the two-channel interference is

$$I \propto [E_t \cos(\omega_t(t)t) + E_r \cos(\omega_r t + \varphi)]^2, \tag{3}$$

where E is the electric field amplitude and φ is the phase between the channels. If we define the optical power measured for each channel as a_r and a_t, then it can be shown that the total measured optical power is

$$P = a_r + a_t + 2\sqrt{a_r a_t}\cos(2\pi\delta(t)t + \varphi), \tag{4}$$

where the measured beat frequency $\delta(t) = v_t(t) - v_r$ is the absolute value of the frequency difference between the two channels. From the beat frequency, the frequency Doppler shift can be extracted as

$$\Delta v_t = |v_{ti} - v_r - \delta|. \tag{5}$$

It is therefore enough to know either v_r and v_{ti} or $|v_r - v_{ti}|$ to extract Δv_t. A standard PDV with no frequency shift is one in which $v_r - v_{ti} = 0$. The target's apparent velocity can be calculated from the calculated Doppler shift using[11]

$$v = \frac{\lambda}{2}\Delta v_t. \tag{6}$$

A basic PDV system includes a laser (usually 1550 nm), a circulator, a coupler, and a detector, as can be seen in the schematic design in Fig. 1.

PDV has several advantages over Line-VISAR, making it at the least an important complementary diagnostic to Line-VISAR. (1) When dealing with temporal resolutions better than 100 ps, PDV potentially has a larger dynamic range than that of existing Line-VISAR. (2) PDV can measure several velocities simultaneously, whereas Line-VISAR cannot. (3) The light interference in PDV is between a reference signal and one that is reflected from the target. While the intensity of the reflected signal is subject to changes in the target's reflectivity, the reference signal is not. Consequently, whereas in Line-VISAR the interference is between two beams reflected from the target, in PDV the reference signal amplifies the interference. Therefore, when comparing systems with similar dynamic ranges, the PDV system can accommodate weaker reflected signals. Note also that because the beating amplitude is proportional to $\sqrt{a_t}$ [see Eq. (4)], the detector can operate in a dynamic range much larger than that allowed by the oscilloscope. (4) Although for short sweep times (1–10 ns) Line-VISAR can provide temporal resolutions of a few picoseconds, the time resolution decreases if the sweep time is increased. In contrast, using a PDV system, very long times (of few microseconds) can be measured with the same time resolution, depending on the oscilloscope parameters.

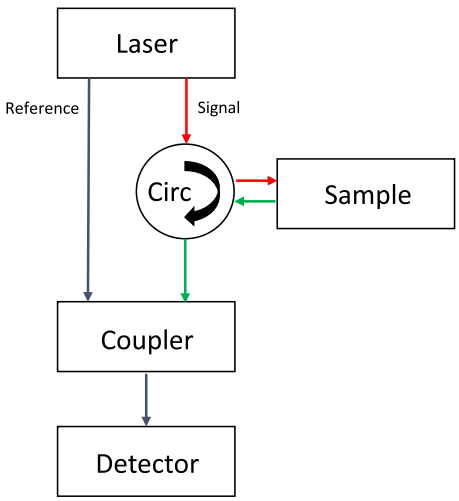

FIG. 1. Basic schematic of photonic Doppler velocimetry (PDV).

III. PDV IMPROVEMENTS FOR SHORT-TIME MEASUREMENTS

A. Increased reference-to-signal intensity ratio

In interferometry, the power ratio of the two signals is usually chosen to maximize the fringe visibility:

$$Vis = \frac{P_{max} - P_{min}}{P_{max} + P_{min}} = \frac{2\sqrt{a_r a_t}}{a_r + a_t}. \tag{7}$$

The fringe visibility has a value between zero and unity, where the maximum visibility is achieved when the two waves have equal power, i.e., $a_r = a_t$, and the minimum visibility is achieved when one of the waves has zero power. However, in an experiment, the signal optical

power reflected from the target usually drops drastically in a very short time period, i.e., the non-oscillating part of the interference signal (i.e., $a_r + a_t$) will decrease drastically as well. In that case, the beating signal might be clipped on the oscilloscope unless a non-optimal scale is chosen on the oscilloscope to prevent such clipping. However, such a non-optimal scale on the oscilloscope will decrease the signal-to-noise ratio and reduce the data quality.

To avoid the aforementioned issues, we chose to increase the reference-channel intensity to its maximum value, which was limited by the detector's parameters. We also decreased the contribution of the target channel by splitting 85% of the reflected intensity from the target to be measured by another detector. This measurement is proportional to the target's reflectivity and will be further discussed later. The remaining 15% was interfered with the reference channel with a reference-to-target ratio of close to 100:1. With such a ratio, even a decrease of an order of magnitude in the reflected light intensity will not decrease the non-oscillating level by much. Meanwhile, increasing the reference intensity keeps the beating amplitude high enough above the noise level. For example, if the reference channel has a 500-mV level and the target channel has a 5-mV level, then the non-oscillating level will be 505 mV and the beating amplitude will be 200 mV (peak to peak). If the noise level is ~10 mV, then the reflected signal must be reduced by a factor of 25 for the beating amplitude to reach the noise level, while at the same time the non-oscillating level will change by less than 5 mV, and thus an optimal scale can be chosen for the oscilloscope such that the initial 200-mV beats cover the entire screen.

B. Reflectivity measurements

The signal reflected from the target was split to have 85% directed to a detector for measuring the reflectivity of the target (see Fig. 3). The reflectivity of the target is an important parameter by itself and can be related to the charge transport properties of the sample. However, it can also be used to help normalize the beating intensity and improve the frequency analysis by evaluating the following equation derived from Eq. (4):

$$\phi(t) \equiv \cos\left(2\pi\delta(t)t + \varphi\right) = \frac{\left(P(t) - a_r - a_t(t)\right)}{2\sqrt{a_r a_t(t)}}. \tag{8}$$

Because $a_t(t)$ is measured and a_r can be extracted from the data, $P(t)$ can be recalculated to avoid the change in intensity by substituting $\phi(t)$ from Eq. (8) back into Eq. (4) while using the measured initial constant value of a_t instead of the measured time-dependent value. Another option is to perform the Fourier transform of $\phi(t)$ directly for analyzing the data. This latter option has an additional advantage of already not including the non-oscillating contributions. Hereinafter, for convenience, we refer to $\phi(t)$ as the normalized PDV signal. Note that to calculate $\phi(t)$ properly, the splitting ratio of the signal from the target reaching each detector (beating and intensity) should be taken into account. Other factors that require further adjustments include any difference in signal losses between the splitter and the detectors, the polarization (see Sec. IV), differences in detector sensitivity, detector biases, and the frequency response of the beating detector, because the intensity of the oscillating contribution can be affected by the change in beats frequency.

Figure 2 shows a simulated PDV signal (black) with $a_r = 0.14$ V, $a_t(0) = 0.014$ V, a starting beats frequency of −10 GHz (the minus sign is set for a shorter reference laser wavelength compared to the target one), and a sudden jump to 3 GHz at $t = 1.5$ ns (simulating sudden movement of the target toward the diagnostic probe), with a gradual linear decrease of the frequency and an exponential decrease of the target reflectivity resulting in a decrease of one order of magnitude in intensity within ~0.7 ns. Gaussian noise of 10% of the beats amplitude has been added to the signal. The simulated intensity data are shown in Fig. 2(b), along with the smoothed intensity, which is used to normalize the signal [shown in Fig. 2(a) in blue]. Figure 2(c) shows the results of the short-time Fourier transform (STFT) of the raw simulated data, depicting the intensity contribution of each frequency as a function of time (spectrogram). The STFT was performed using 1500 bins, a Hann window of 80 data points (1 ns), and a single data point between the start times of consecutive windows. The red line in Fig. 2(c) shows the frequency with the maximum intensity contribution for each t within a region of interest (ROI) that excludes $f = 0$ and is called the frequency (velocity) profile. Figure 2(d) similarly shows the spectrogram and frequency profile for the normalized PDV

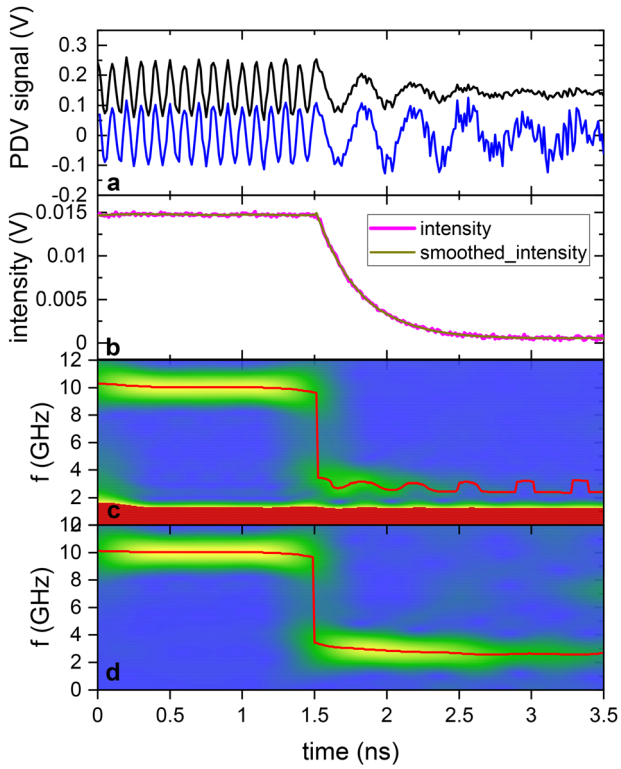

FIG. 2. (a) Simulated raw PDV signal with Gaussian noise of 10% of the beats amplitude (black), and normalized PDV signal (blue). The signal represents a starting frequency of −10 GHz with a sudden change to 3 GHz at 1.5 ns, followed by a slow decrease in frequency and an exponential decrease in target signal intensity. (b) Simulated intensity data with Gaussian noise (magenta), and smoothed intensity data (dark yellow). (c) Short-time Fourier transform (STFT) of simulated signal loses most of the intensity by 2.5 ns (within ~1 ns of the change), and the frequency profile obtained from finding the maximum intensity at each time-point fluctuates. (d) STFT of normalized signal shows that most of the intensity is kept up to 3.5 ns (an additional 1 ns compared to the raw signal) and that the obtained frequency profile does not fluctuate significantly.

signal. It is clear from comparing Figs. 2(c) and 2(d) that normalization provides two benefits in this case: (i) the signal is visible for ~1 ns longer (up to 3.5 ns, compared to ~2.5 ns) and (ii) the obtained frequency profile fluctuates much less.

IV. EXPERIMENTAL SETUP

A. Improved PDV setup

The PDV comprised the following components as shown in Fig. 3. The lasers used had a DC power of up to 1 W at 1550.12 nm with a tunability of approximately ±500 pm and a linewidth of less than 15 kHz. On the target channel, a fast optical switch was used to avoid heating the sample prior to the experiment, and a narrowband filter was placed to block unwanted light returning from the sample.

Usually in PDV systems, the optical path of the light along the reference and target channels is not polarization maintaining, therefore the measured beating intensity is very sensitive to any bending in the optical fibers or changes in the reflected light from the target that may change the light polarization.

In the present experiments, it was found that adding a fiber polarization controller at the end of each of the reference and target channels, as can be seen in Fig. 3, could reduce the polarization sensitivity dramatically. To obtain the maximum possible beating amplitude, we adopted the following procedure: (i) adjust the fiber polarization controller on the reference channel to obtain the maximum non-oscillating signal level; this step is necessary because in general the polarization can be elliptical; (ii) adjust the fiber polarization controller on the target channel to obtain the maximum beating amplitude.

B. Targets, drive laser, and detectors

The improvements presented above were tested in a series of laser-shock experiments, and typical results will be presented. The targets used for the experiment were commercial Au foils of thickness 10, 15, 20, 30, and 40 μm. The surface roughness of the 15-μm foil was measured to be $Ra = 0.175\ \mu$m and $Rz = 2.7\ \mu$m, and it was noticed that in general the thicker the foil, the better the surface roughness.

The experiments were conducted at the National Laser Facility (NLF) in Soreq, using one of its main beams as the drive laser. The drive laser was a frequency-tripled Nd:glass laser that produced 351-nm light.

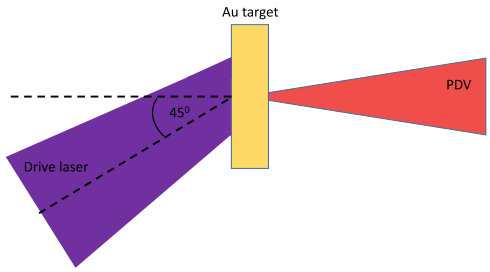

FIG. 4. Target alignment setup.

One of two lens arrays was selected to form a laser focal spot with a flat-top diameter of either 400 or 600 μm. However, the beam was incident at 45° to the target's surface, as can be seen in Fig. 4, resulting in a larger and elliptical effective spot size. The pulse temporal shape was a super-Gaussian nearing a top hat with a pulse duration of 1–3 ns. The PDV probe was an OZ Optics LPF-04-1550-9/125-S-5-112-18AS-60-3A-1-0.6 Pigtail Style Focuser with a single-mode fiber, an 8-mm collimator, and a 112-mm working distance, producing a focal spot of 70 μm in diameter. The probe was aligned nearly vertically to the target surface, as can be seen in Fig. 4.

We used a Thorlabs PDA8GS detector for the PDV signal, with a sensitivity of −20 dBm and a maximum peak power of 20 mW (dynamic range up to 2000:1). This detector can nominally be used up to 9 GHz, but beats of up to ~15 GHz can be observed with it, albeit with a significant decrease of intensity starting above ~8 GHz. The intensity was measured using a Newport AD-40APDir detector with a sensitivity of −27 dBm and a maximum average power of 5 mW (dynamic range of at least 2500:1). The oscilloscope used in this experiment had a bandwidth of 33 GHz, and so our bandwidth was limited by the PDV detector.

V. RESULTS

Figure 5(a) shows the PDV signal collected from shot EOS3-S09 (160 J, 1 ns, 650 μm spot diameter) on a 40-μm Au foil (black) with $a_r \approx 0.24$ V, $a_t(0) \approx 0.004$ V, and a starting beats frequency of 1.16(1)

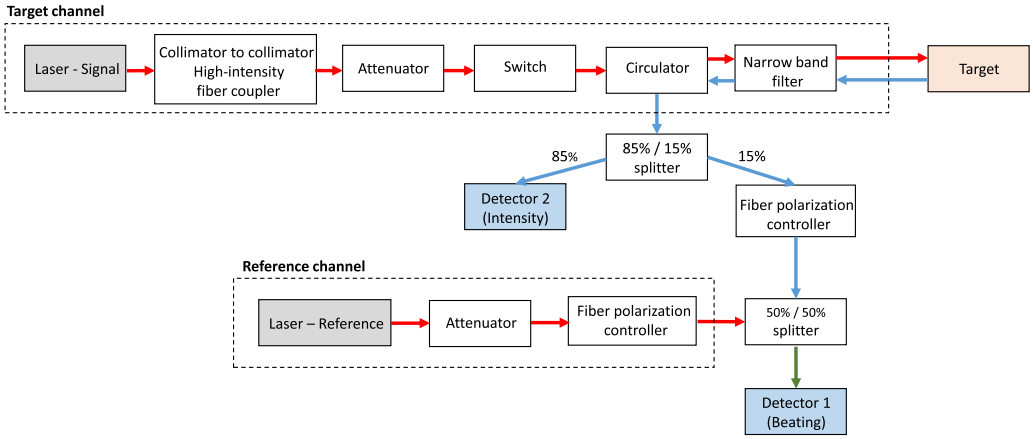

FIG. 3. Schematic of PDV.

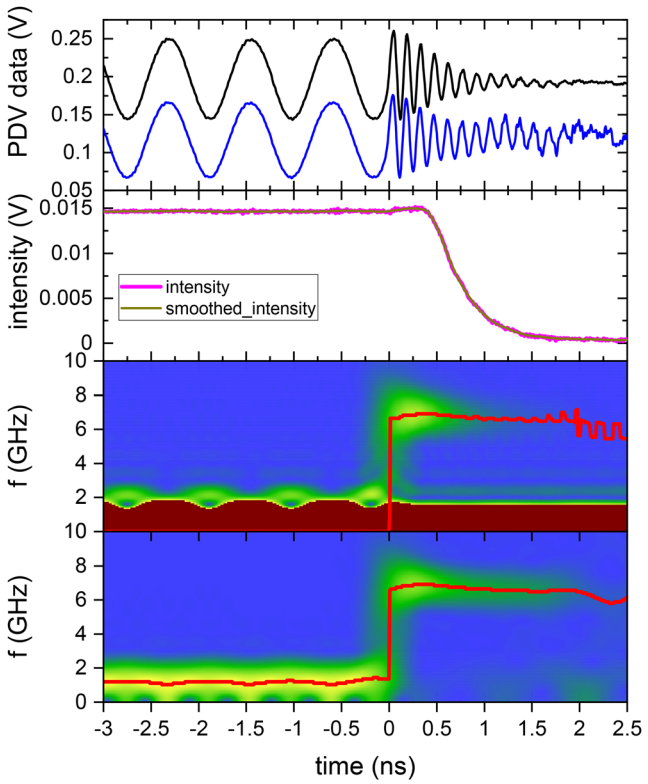

FIG. 5. Shot EOS3-S09. (a) Raw PDV signal collected from a 40-μm Au foil (black), and normalized PDV signal (blue, shifted). The reference channel was set to start with beats of 1.16 GHz. (b) Measured intensity data (magenta) and smoothed intensity data (dark yellow). Note that a different detector was used for the intensity measurement and hence the difference in voltage scales (c) STFT of raw PDV signal (using a Hann window of 1 ns and 1500 bins) loses almost all of the intensity by 1 ns, and the frequency profile (red) obtained from finding the maximum intensity at each time-point fluctuates. Dark red represents values above the set upper limit. (d) STFT of normalized signal shows that enough intensity is kept up to ~2 ns (an additional 1 ns compared to the raw signal) and that the obtained frequency profile does not fluctuate significantly. Note that the beats of the initial frequency of 1.16 GHz are spaced apart at intervals very close to the 1 ns of the FFT window, resulting in slightly different contributing frequencies at different window positions, which leads to fluctuations in the frequency with the most significant contribution, even following normalization. The reported initial frequency value was obtained using a fit to a duration of several nanoseconds. It is possible to use a wavelet transform instead of an STFT to prevent fluctuations in low-frequency contributions.

GHz. An oscilloscope with a sampling rate of 128 GSa/s was used. We mark $t_0 = 0$ as the point when a change in frequency is observed, coinciding with the start of a very slight and gradual increase in measured intensity [Fig. 5(b), magenta], followed by a strong, nearly exponential, decrease in intensity [Fig. 5(b)]. This t_0 is defined as the start of motion of the free surface. The smoothed intensity [Fig. 5(b), dark yellow] is used to obtain $\phi(t)$ according to Eq. (8) and is shown in Fig. 5(a) (blue). The normalization in the experimental examples given here is not perfect because we correct for the change in reflectivity but not for changes in the detector response to the frequency change, nor to possible changes in polarization, and possibly other effects. The STFT [using a Hann window of 1 ns (see the Appendix for a comparison when using a 4-ns window), one data point between the start of consecutive windows, and 1500 bins] of the raw PDV signal is shown in Fig. 5(c), and the STFT of the normalized PDV signal is shown in Fig. 5(d), with the red line in each panel showing the obtained frequency profile by finding the maximum value within an ROI. It is clear that following normalization, as in the case of the simulated data, the intensity in the spectrogram can be seen well for ~1 ns longer, and that the obtained frequency fluctuates significantly less.

The maximum frequency observed, at ~200 ps after the start of motion, is $f = 6.9(1)$ GHz, and when taking into account the initial beats frequency of $f_0 = 1.16(5)$ GHz and the laser wavelength $\lambda = 1550.12$ nm, we obtain using Eq. (6) a free-surface velocity of

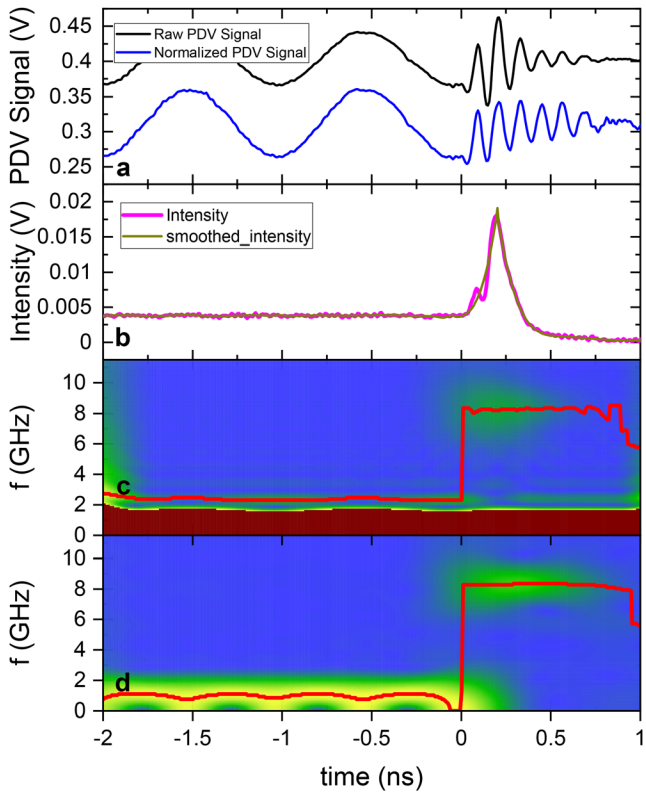

FIG. 6. Shot EOS3-S15. (a) Raw PDV signal collected from a 20-μm Au foil (black), and normalized PDV signal (blue, shifted). The reference channel was set to start with beats of −1.02 GHz. (b) Measured intensity data (magenta) and smoothed intensity data (dark yellow). Note that a different detector was used for the intensity measurement and hence the difference in voltage scales (c) STFT of raw PDV signal (Hann window of 1 ns, with 1500 bins) loses almost all of the intensity by ~0.55 ns, and the frequency profile (red) obtained from finding the maximum intensity at each time-point fluctuates. Dark red represents values above the set upper limit. (d) STFT of normalized signal has better intensity up to ~0.75 ns (an additional 0.2 ns compared to the raw data), and the signal fluctuates significantly less. Note that the beats of the initial frequency of 1.02 GHz are spaced apart at intervals very close to the 1 ns of the FFT window, resulting in slightly different contributing frequencies at different window positions, which leads to fluctuations in the frequency with the most significant contribution, even following normalization. Without normalization, we observe a frequency above 2 GHz, which is an artifact of the FFT window [other frequencies can also be seen in panel (c)].

u_{fs} = 4.5(1) km/s. The velocity decreases slowly, reaching 4.2(1) km/s at ~1.5 ns after the movement begins.

The error estimate for the maximum observed frequency is based on the change we observe in the maximum frequency when choosing a different window size in the STFT. According to the uncertainty principle, we have[4]

$$\Delta f \cdot \tau \geq \frac{1}{4\pi}, \tag{9}$$

which for a window of 1 ns results in $\Delta f \sim 0.08$ GHz ($\Delta v \sim 62$ m/s). This uncertainty represents the limit of the ability to distinguish between two or more concurrent frequencies contributing to the total signal. As determined by Dolan,[2] the lower limit for the uncertainty of a single frequency is ~10 m/s for a 1-ns window and a −40-dBm light return level. The larger uncertainty obtained in this experiment is due to either a distribution of velocities or the fact that the velocity changes over time, even within the 1-ns window, effectively creating a frequency distribution within the window. In general, the error estimate of the initial beats frequency is much smaller because it is possible to fit the data to a sine wave or perform a fast Fourier transform (FFT) with a longer window and obtain a more precise value. We therefore conclude that the actual error of the free-surface velocity is in the range of 10–100 m/s; a more detailed error analysis (such as that presented by Dolan[11]) might narrow this range. Note that it is possible that the value obtained through the STFT is indeed the maximum velocity, but there is also the possibility that the actual maximum velocity occurs at an earlier time and that because of the 1-ns window, we observe a lower velocity in the first 200 ps.

Using the maximum free-surface velocity u_{fs} = 4.5(1) km/s and assuming $u_{fs} \approx 2u_p$, the shock velocity u_s = 6.62(18) km/s and pressure P = 2.85(12) Mbar were calculated according to the equation of state reported by Yokoo *et al.*:[12]

$$u_s = 2.995 + 1.653\,(56)u_p - 0.013\,(19)u_p^2 \tag{10}$$

and using an initial density of Au of $\rho_0 = 19.3$ g/cm^3. Figure 6(a) shows the PDV signal collected from shot EOS3-S15 (83 J, 1 ns, 400 μm) on a 20-μm Au foil (black) with $a_r \approx 0.4$ V, $a_t(0) \approx 0.004$ V, and a starting beats frequency of −1.02(1) GHz (the minus sign is set for a shorter reference wavelength). We mark the start of motion as $t_0 = 0$, where a change of frequency is observed, along with an increase in intensity [Fig. 6(b)], followed by a nearly exponential decrease in intensity, with almost no intensity left at ~0.55 ns after the start of motion begins. The STFTs of the raw PDV signal and the normalized PDV signal are shown in Figs. 6(c) and 6(d), respectively, along with the frequency profiles (red lines). For this case of a higher frequency after the shock breakout, compared to EOS3-S09, the effect of normalization is not as significant, possibly because of having a larger number of complete cycles within the 1-ns STFT window, which then requires less intensity for a reasonable result.

The maximum frequency observed, immediately following the start of motion, is 8.3(1) GHz, resulting in u_{fs} = 7.3(1) km/s. Using the maximum free-surface velocity u_{fs} = 7.3(1) km/s, the shock velocity u_s = 8.9(3) km/s and pressure P = 6.2(3) Mbar were calculated according to the equation of state reported by Yokoo *et al.*[12]

VI. CONCLUSION

As presented herein, the improvements to standard PDV allow the free-surface velocity of opaque materials to be measured in the terapascal pressure range. This paper presents results of the free-surface velocity of Au up to a shock pressure of ~7 Mbar with an error of less than 1.5% in u_{fs} = 7.3 km/s. Note also that in all our measurements, we observed a single velocity at short times (a few nanoseconds) after shock breakout, while at long times (a few hundred nanoseconds) after shock breakout we observed a cloud of debris with a velocity spread centered at the free-surface velocity. Although discussing the debris cloud is beyond the scope of this paper, we see it as an indication that the free surface did not break for the measurement times discussed herein.

Because the main diagnostic in current laser shock experiments is Line-VISAR, which is limited to measuring the free-surface velocity of opaque materials up to ~1 Mbar, this makes PDV a valuable complementary diagnostic in such experiments along with several other advantages over Line-VISAR. We expect the free-surface velocity measurements with PDV to be extended to much higher pressures, mainly by adjusting the beating frequency to higher frequency to allow for more beatings in the short measurement time. We also predict that the measurement error could be reduced by applying an analysis more suitable to short alternating signals, such as the wavelet transform instead of the STFT.

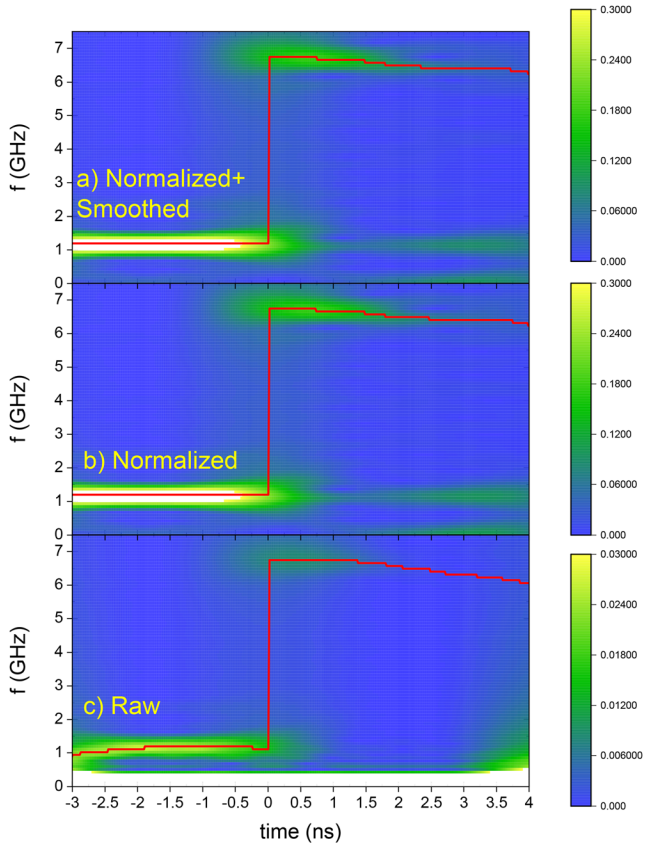

FIG. 7. STFT of EOS3-S09 using a sliding window of 512 data points (4 ns) following (a) normalization by a smoothed intensity measurement, (b) normalization by the raw intensity measurement, and (c) no normalization. White represents values above the set maximum value. Red lines are the maximum contribution to the frequency at each time and represent the frequency profile.

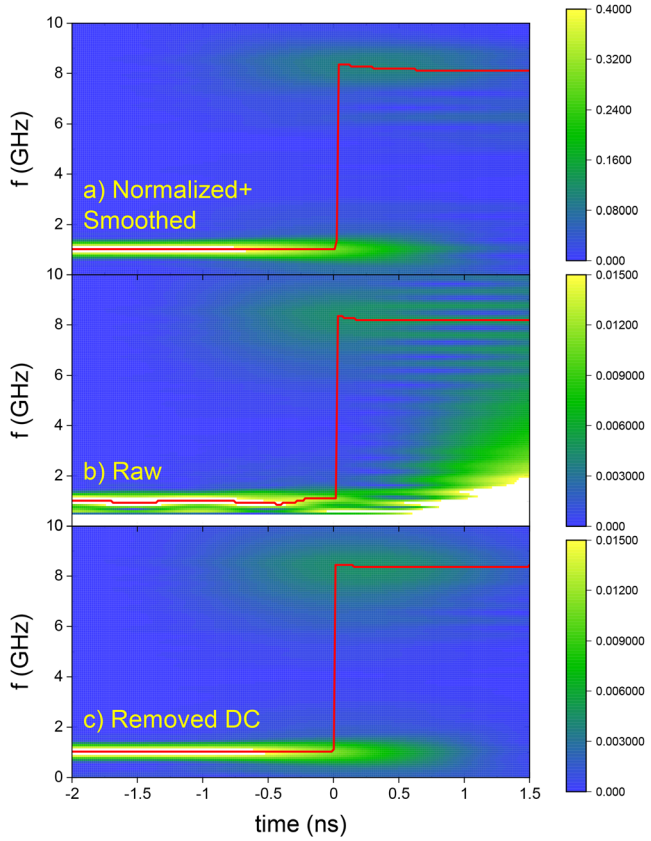

FIG. 8. STFT of EOS3-S15 using a sliding window of 512 data points (4 ns) following (a) normalization by a smoothed intensity measurement, (b) no normalization, and (c) removal of the DC component. White represents values above the set maximum value. Red lines are the maximum contribution to the frequency at each time and represent the frequency profile.

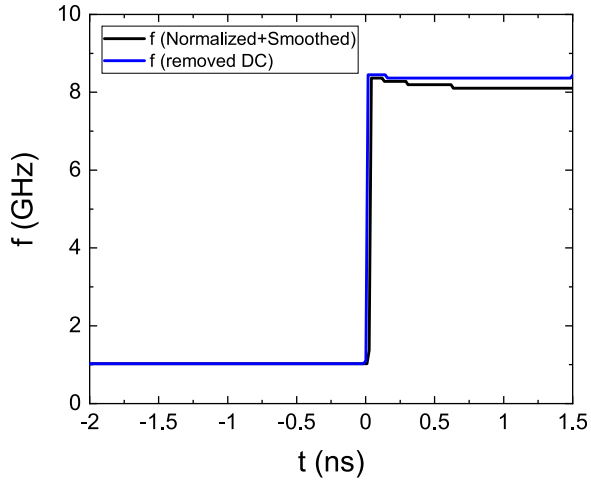

FIG. 9. Frequency profile obtained for EOS3-S15 using a sliding window of 512 data points (4 ns) following normalization (black) compared to following removal of the DC signal (blue).

APPENDIX: NOTES ON FFT ANALYSIS

We provide here figures comparing various analysis conditions using a large window of 512 data points (4 ns) for shot EOS3-S09 (Fig. 7). Note that the smoothing we use is only for the intensity measurement and not the PDV measurement, with the purpose of not introducing additional noise, and it has very little effect on the obtained spectrogram and the frequency profile [compare Figs. 7(a) and 7(b)]. Using a 4-ns window, compared to the 1-ns window in the main text, allows us to observe the velocity at longer times even without using the intensity data for normalization. However, this does not allow us to properly observe changes over time. Note further that when using a 4-ns window, for the normalized data we observe a velocity even up to 4 ns, but upon further inspection of the spectrogram we can see that above 2 ns there are actually two branches of frequencies (in addition to a remnant of the original frequency before the shock breakout, which is due to an internal reflection), meaning that this is probably an artifact of the Fourier analysis and that even if there is any signal there, it is too weak to obtain a reliable value.

We provide another example here for EOS3-S15 (Fig. 8), where we observe that without normalization there are significant artifacts emanating from the DC component [the non-interfering components in Eq. (3); see Fig. 8(b)], and that by removing the DC component the spectrogram is quite similar to the one obtained following normalization [Fig. 8(c)]. However, note that the frequency profile without normalization does exhibit differences; namely, it appears constant, whereas following normalization we observe a decrease in frequency with time. This difference can be seen more clearly in Fig. 9. This is most likely due to having a larger amplitude immediately following the breakout. Therefore, when using a large FFT window and having a much smaller amplitude at later times, this strong contribution at earlier times still has a large effect.

REFERENCES

[1]O. T. Strand, D. R. Goosman, C. Martinez, T. L. Whitworth, and W. W. Kuhlow, "Compact system for high-speed velocimetry using heterodyne techniques," Rev. Sci. Instrum. **77**(8), 083108 (2006).

[2]D. H. Dolan, "Extreme measurements with photonic Doppler velocimetry (PDV)," Rev. Sci. Instrum. **91**(5), 051501 (2020).

[3]B. J. Jensen, F. J. Cherne, and N. Velisavljevic, "Dynamic experiments to study the $\alpha - \varepsilon$ phase transition in cerium," J. Appl. Phys. **127**(9), 095901 (2020).

[4]B. J. Jensen, D. B. Holtkamp, P. A. Rigg, and D. H. Dolan, "Accuracy limits and window corrections for photon Doppler velocimetry," J. Appl. Phys. **101**(1), 013523 (2007).

[5]G. D. Stevens *et al.*, "Free-surface optical scattering as an indicator of the shock-induced solid-liquid phase transition in tin," J. Appl. Phys. **104**(1), 013525 (2008).

[6]S. Eliezer, *The Interaction of High-Power Lasers with Plasmas* (Institute of Physics Publishing, Bristol, 2002).

[7]L. M. Barker and R. E. Hollenbach, "Laser interferometer for measuring high velocities of any reflecting surface," J. Appl. Phys. **43**(11), 4669–4675 (1972).

[8]P. M. Celliers, G. W. Collins, L. B. Da Silva, D. M. Gold, and R. Cauble, "Accurate measurement of laser-driven shock trajectories with velocity interferometry," Appl. Phys. Lett. **73**(10), 1320–1322 (1998).

[9]P. M. Celliers, D. K. Bradley, G. W. Collins, D. G. Hicks, T. R. Boehly, and W. J. Armstrong, "Line-imaging velocimeter for shock diagnostics at the OMEGA laser facility," Rev. Sci. Instrum. **75**(11), 4916–4929 (2004).
[10]D. H. Dolan *et al.*, "Tracking an imploding cylinder with photonic Doppler velocimetry," Rev. Sci. Instrum. **84**(5), 055102 (2013).
[11]D. H. Dolan, "Accuracy and precision in photonic Doppler velocimetry," Rev. Sci. Instrum. **81**(5), 053905 (2010).
[12]M. Yokoo, N. Kawai, K. G. Nakamura, K. Kondo, Y. Tange, and T. Tsuchiya, "Ultrahigh-pressure scales for gold and platinum at pressures up to 550 GPa," Phys. Rev. B **80**(10), 104114 (2009).